A COMPARISON OF COMPUTER-GENERATED LIFT AND DRAG POLARS FOR A WORTMANN AIRFOIL TO FLIGHT AND WIND TUNNEL RESULTS

CB 609194

FINAL REPORT

PRINCIPAL INVESTIGATORS

Albion Hideto Bowers

Doral R. Sandlin

June 1984

California Polytechnic State University

Aeronautical Engineering Department

San Luis Obispo, California

TABLE OF CONTENTS

Table of Contents	.....	ii
Abstract	.....	iii
List of Symbols	.....	iv
List of Tables	.....	v
List of Figures	.....	vi
Introduction	.....	1
Experimental Background	.....	4
Analytic Background	.....	7
Discussion of Results	.....	9
Concluding Remarks	.....	15
Appendix	.....	17
References	.....	18
Tables	.....	20
Figures	.....	24

A COMPARISON OF COMPUTER-GENERATED LIFT AND DRAG POLARS FOR A WORTMANN AIRFOIL TO FLIGHT AND WIND TUNNEL RESULTS

Albion Hideto Bowers

June 1984

Computations of drag polars for a low-speed Wortmann sailplane airfoil are compared to both wind tunnel and flight results. Excellent correlation is shown to exist between computations and flight results except when separated flow regimes were encountered. Wind tunnel transition locations are shown to agree with computed predictions. Smoothness of the input coordinates to the PROFILE airfoil analysis computer program was found to be essential to obtain accurate comparisons of drag polars or transition location to either the flight or wind tunnel results.

LIST OF SYMBOLS

C_l	section lift coefficient, $2L/pv_o^2S$
C_d	section drag coefficient, $2D/pv_o^2S$
R	Reynolds number, pvc/m
d_2	momentum thickness, $v/v_o(1-v/v_o)dy$
d_3	energy thickness, $v/v_o(1-(v/v_o)dy$
H_{32}	shape factor, d_3/d_2
Rd_2	local Reynolds number based on d_2, pvd_2/m
x/c	nondimensional chord length
z/c	nondimensional vertical length
a	angle of attack, deg.
C_p	pressure coefficient, $(P-P_o)/q_o$
q_o	free stream dynamic pressure, $pv_o^2/2$
q	dynamic pressure, $pv^2/2$
P_t	free stream total pressure, P_o+q_o
P_t	total pressure, P+q
v_o	free stream velocity
v	velocity
P_o	free stream static pressure
P	static pressure
c	chord

LIST OF TABLES

Table 1	Coordinates of Design FX61-163 Airfoil
Table 2	Coordinates of Measured Flight T-6 Airfoil
Table 3	Coordinates of Model FX66-17AII-182 Airfoil
Table 4	Coordinates of Smoothed Flight T-6 Airfoil

LIST OF FIGURES

Fig. 1	3 view of T-6 sailplane
Fig. 2	Comparison of FX61-163 and T-6 airfoils
Fig. 3	Flight wake rake installation
Fig. 4	T-6 section C_l vs. R graph
Fig. 5	T-6 section C_l vs. C_d flight polar
Fig. 6	T-6 wind section wake profile
Fig. 7	Computed pressure coefficients of Model FX66-17AII-182
Fig. 8	Computed pressure coefficients of flight T-6 airfoil
Fig. 9	Computed pressure coefficients of SLOPE and MOD T-6 by SLOPE and MOD
Fig. 10	Computed pressure coefficients of SMOOTH T-6 by SLOPE, MOD and hand
Fig. 11	Comparison T-6 analytic polars, smoothed and unsmoothed
Fig. 12	Comparison of wind tunnel and computed FX66-17AII-182 transition
Fig. 13	Comparison of wind tunnel and computed FX61-163 polars
Fig. 14	Comparison of flight T-6 and computed polars

Chapter 1

INTRODUCTION

In the interest of keeping costs down, computational methods, rather than wind tunnel and flight tests, are being used more extensively to predict performance and handling characteristics of aircraft. Of primary importance are airfoil parameters. It is therefore of interest to establish the regime of validity of computational methods for design and analytic purposes by comparing results of flight, wind tunnel, and analytic methods.

Inviscid incompressible flow fields have been analytically produced since just after the turn of this century, (ref 1 and ref. 2). This allowed pressure coefficient data to be created resulting in lift coefficient estimation. Until the 1960's, considerable interest in increasing flight velocities resulted in a minimal amount of work being done in the low speed, low Reynolds number area. At the same time viscous effects were being investigated and modeled from both empirical and analytical investigations.

The sailplane community has provided the most information on airfoils in the largely unknown low Reynolds number range. F. X. Wortmann and D. Althaus have provided comprehensive wind tunnel data on numerous low speed airfoils, (ref. 3). The University of Stuttgart, West Germany and NASA Langley Research Center developed a computer program called PROFILE to design and analyze incompressible, viscous performance parameters on airfoils, (ref. 4). In 1973 and 1974, flight tests were performed on a T-6 sailplane at NASA Ames Research Center, Dryden Flight Research Facility to determine in-flight drag polars, (ref. 5).

This study will present comparisons of these data in order to ascertain the validity of the PROFILE program in predicting transition, lift, and drag polars on a sailplane airfoil.

The results of this report will be used to build a body of knowledge in the area of low Reynolds number aerodynamics with potential application in high altitude "poor man's satellite" drones or atmospheric samplers.

Analytic data were produced at Reynolds number of 1×10^6, 1.3×10^6, 2×10^6, and 3×10^6 to correspond with the speed range of the flight data. All airfoils were extensively smoothed to minimize waviness sensitivity in the program.

Chapter 2

EXPERIMENTAL BACKGROUND

Wind Tunnel Tests

For this report, wind tunnel results were used to correlate computational results for both drag polar data and transition location. Wind tunnel drag polar data were available, (ref. 3), for an airfoil similar to the flight airfoil--the Wortmann FX61-163. Since transition wind tunnel data were not available for an airfoil similar to this, computational data were correlated with a Wortmann FX66-17AII-182 airfoil.

An investigation was conducted at Langley Research Center to empirically determine the characteristics of a Wortmann FX66-17AII-182 airfoil as manufactured on a fiberglass sailplane, (ref. 6). Wing pressure coefficient and transition data were obtained in the low-turbulence pressure tunnel.

Transition was determined by two methods. Oil-flow photographs were taken of the upper surface during tests, and transition points were plotted. This was done by painting oil on the wing surface and observing the patterns the airflow created. A stethoscope connected to various pressure ports on the airfoil was used to determine approximate transition location by listening for the large increase in noise level that occurs after transition.

Flight Tests

In 1974, the joint NASA-SSA (Soaring Society of America) report was published containing results of airfoil section drag measurements taken in flight. This was accomplished with a pitot probe traversing a wing wake and utilizing Jones' method of momentum deficit, (ref. 7 and in the appendix). The T-6 sailplane (fig. 1) used a modified Wortmann

FX61-163 airfoil. The design (Table 1) and actual flight airfoils (Table 2) differed considerably on the lower surface near the trailing edge (fig. 2).

The wake rake installation, (fig. 3), included a trailing static probe for free stream static pressure; a Kiel tube for free stream total pressure; a radially traversing pitot-static probe located 0.32c behind the trailing edge; and a pressure transducer that was switchable to each pressure port.

Flight tests were conducted between airspeeds of 40 and 125 knots. Due to the fixed wing loading of the test vehicle a particular lift coefficient corresponded to a specific Reynolds number (fig. 4). The Reynolds number range was from 1×10^6 to 3×10^6. A polar from these tests is shown (fig. 5) followed by a sample wing wake (fig. 6).

Chapter 3

ANALYTIC BACKGROUND

The results of a computer program by the name of PROFILE (ref. 1) were used in this study to compare with the experimental data. PROFILE was first developed in the early 1960's and has been updated every two years. The latest version can be divided into two parts during analysis. The first part is strictly inviscid and is used for pressure coefficient calculations. The second half computes all viscous effects.

The inviscid portion determines the pressure coefficient or velocity distribution on the airfoil. This is accomplished using a vortex panel method with parabolically

distributed source-sink singularities on a cubic spline fitted curve through the coordinate points. An example of the model airfoil is given, (fig. 7).

The viscous portion uses the specified values of Reynolds number and computes transition and separation characteristics. A boundary-layer development, consisting of displacement, momentum, and energy thickness (d_1, d_2, and d_3), can be specified.

Location of transition is a function of the shape factor H_{32} and local Reynolds number based on momentum thickness Rd_2. No roughness was used in the program as all airfoils tested were essentially smooth, and natural transition was assumed. H_{32} is computed as a function of both the arc length from the trailing edge and the pressure gradients. The criteria used for transition was developed in ref. 8 and laminar flow is assumed in eq. 1:

$$\ln(Rd_2) \geq 18.4(H_{32}) - 21.78 \qquad (1)$$

Criteria for separation is not as well defined as for transition. Usually turbulent separation is presumed to have occurred when H_{32} falls below 1.46. A more involved look at separation criteria is given in ref. 9.

Chapter 5

DISCUSSION OF RESULTS

Computational Results

PROFILE was used to analytically predict lift and drag polars for the design and flight (sailplane) FX61-163 airfoils (tables 1 and 2). In addition, predictions of transition criteria and pressures were obtained for comparison to the results of the model (wind tunnel) airfoil FX66-17AII-182 of Table 3.

The PROFILE program required considerable smoothing of the flight FX61-163 airfoil for full "drag bucket" development. The airfoil was considered smooth when the inviscid pressure distribution was smooth. The raw data airfoil coordinates produced a very erratic inviscid pressure coefficient distribution, fig. 8. The primary coordinate-smoothing programs SLOPE and MOD were used to ensure that the analyzed airfoil maintained close geometric characteristics of the flight airfoil. Even after using SLOPE and MOD, hand-smoothing was necessary to satisfy PROFILES's input requirements for smooth coordinates.

SLOPE would output the slopes of the lines connecting each coordinate point. These slopes were then plotted as a function of x/c and a new faired curve was drawn through the points to obtain new slope values.

The new slope values were then fed into the MOD program and new z/c coordinates were produced. The resulting airfoil was then visually inspected to verify the airfoil had not been unduly modified with respect to thickness, thickness distribution, camber, and trailing edge thickness (the leading edge is normally left alone).

The resulting airfoil pressure distributions were analyzed (fig. 9) and it was determined that more smoothing was required. Final smoothing was done by changing z/c coordinates by hand-fairing to obtain the final airfoil (fig. 10 and Table 4). Final changes to the airfoil coordinates were

about 0.002 inch for a 30 inch chord. It should be emphasized that the level of smoothness is artificially high due to sensitivity in the program.

For the flight airfoil, the maximum deviation from the mean in the airfoil corresponded to .020 inch over a 2.0-inch length while waviness of less than .001 inch over 2.0 inches could be seen readily. A comparison of the computed lift and drag polars for each smoothing step is shown (fig. 11) for $R = 1 \times 10^6$ and $-4^o < a < 14^o$. A comparison of the airfoil polars for various degrees of smoothness (figs. 8, 9, and 10) will provide some insight into the PROFILE program. All three airfoils produce nearly identical drag coefficients between lift coefficients of 0.12 and 0.66. Above and below these lift coefficient values the raw data T-6 airfoil is predicted to have leading-edge transition, with no appreciable increase in separated flow causing a rise in drag. Beyond a lift coefficient value of approximately 0.85, the upper surface separation increases markedly causing the drag to rise.

The SLOPE- and MOD-smoothed airfoil shows a drag bucket extending from -0.04 to 0.92 lift coefficient. Transition then causes an increase in drag without loss of lift. The C_l nearly reaches 1.0 before separation causes loss of lift and increased drag. The final SMOOTH airfoil's drag bucket

extends from C_l = -0.09 to 1.0. In this case the increasing angle of attack causes drag rise due to the onset of leading edge transition and separation, simultaneously.

The final SMOOTH airfoil polar is shown at R = 1.0 x 10^6, 1.3 x 10^6, 2.0 x 10^6, and 3.0 x 10^6 (fig. 13). This is the analytic result that will be compared with the flight polar. The design FX61-163 airfoil was also analyzed for comparison and no smoothing was required on its coordinates.

Comparison of Results

When the wind tunnel FX66-17AII-182 model C_p values, figure 12, are plotted on the PROFILE predictions, only a slight deviation occurs near the transition region and at the trailing edge. At these two points viscous effects alter the C_p data in the wind tunnel. The C_p rises slightly above the prediction at the trailing edge due to the inviscid prediction's complete pressure recovery.

As shown in figure 12, PROFILE's accuracy in predicting transition was very good; within 0.5 percent of chord length, which was typical of all analyzed cases.

Comparison of the wind tunnel design airfoil with PROFILE, figure 13, shows marginally lower section drag at section lift coefficients lower than 1.15 at R = 2.0 x 10^6 and 3.0 x 10^6. This comparison is considered to be a very good correlation in that wind tunnel accuracies between tests are usually not better than 3 percent. At R = 1 x 10^6, PROFILE's correlation is not as good. The wind tunnel polar exhibits a characteristic of a probable laminar separation bubble which PROFILE would be unable to predict accurately. Smoothing of the airfoil coordinates in this case would not improve the correlation as laminar separation bubbles are not accurately predicted and the airfoil coordinates had already been smoothed.

When PROFILE is compared to flight results, figure 14, extremely good correlation is found at Reynolds number of 3 x 10^6 and 2 x 10^6 corresponding to lift coefficients of 0.14 and 0.32, respectively. Flight data indicates slightly less section drag than predicted but approximately equals the program variations ($\pm$ 0.0001 in drag coefficient). At Reynolds number of 1.3 x 10^6, the correlation deteriorates and continues to do so approaching R = 1.0 x 10^6. At R = 1.3 x 10^6, drag coefficient is predicted to be 0.0010 higher than actually found in flight measurements. Although the T-6 sailplane never quite achieved a C_l of 1.38 corresponding to

a R of 1.0×10^6, 1.10×10^6 was considered to be representative. PROFILE predicts the drag coefficient to be 0.0207 and 0.0197 at a lift coefficient of 1.047 and 1.039 at 1×10^6 and 1.3×10^6 Reynolds number, respectively, while the flight airfoil at a C_l of 1.15 has a C_d of 0.0140. It is possible that additional smoothing might improve the correlation at these high C_l's.

Chapter 5

CONCLUDING REMARKS

Several airfoils were analyzed using PROFILE and compared with both wind tunnel and in-flight experimental results. Excellent correlation was shown to exist at moderate to high ($2 \times 10^6 \geq R \geq 3 \times 10^6$) Reynolds numbers and low to moderate lift coefficients ($0.1 \geq C_l \geq 0.8$). At low Reynolds numbers ($<1.3 \times 10^6$) and higher C_l's (> 0.8) the correlations deteriorated. These areas were usually found to have some degree of separated flow. Intensive smoothing of airfoil coordinates improved the correlation. However, it is possible that if the airfoils analyzed were even smoother, better correlation may have been possible. This degree of smoothness is

required for good results from PROFILE, but is not necessary for high performance in flight. The use of SLOPE and MOD with judicious hand-smoothing was needed to ensure that the analytic airfoil maintained a good geometric likeness to the flight airfoil.

This limited study indicates that present analytic methods exhibit good correlation, except in low Reynolds number (1.0×10^6) and high C_l (> 0.8) regimes.

Appendix

Experimental method due to Jones. Jones' equation is given in ref. 7 as:

$$C_d = \frac{2}{c} \quad \frac{P_t - P}{q} \quad (1 - \frac{P_t - P_t}{q}) dy$$

where:

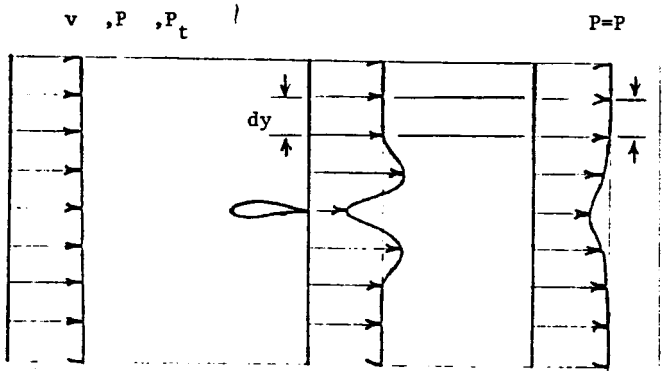

Free Stream Wing Station Measurment Station

since:

$$P_t - P_t = q + P$$

substituting:

$$C_d = \frac{2}{c} \quad \frac{q}{q} \quad (1 - \frac{q + P}{q}) dy$$

REFERENCES

1. O. Blumenthal and E. Trefftz. Pressure Distributions on Joukowski Wings and Graphic Construction of Joukowski Wings. Zeit Schrift fur Flugtechnik und Motorluft Schiffahrt, 1913.

2. T. Theodorson and I. E. Garrick. General Potential Theory of Arbitrary Wing Sections. NACA TR No. 452, 1933.

3. D. Althaus and F. Wortmann. Stuttgarter Proflikatalog 1. Braunschweig, Wiesbaden. Vieweg, 1981.

4. R. Eppler and D. Somers. A Computer Program for the Design and Analysis of Low Speed Airfoils. NASA TM 80210, 1980.

5. L. Montoya; P. Bikle; and R. Banner. Section Drag Coefficients from Pressure Probe Traverses of a Wing Wake at Low Speeds. Advanced Technology Airfoil Research - Vol. 1, NASA CP 2045, Part 1, 1979 (pp. 601-622).

6. D. Somers. Experimental and Theoretical Low Speed Aerodynamic Characteristics of a Wortmann Airfoil as Manufactured on a Fiberglass Sailplane. NASA TND-8324, 1977.

7. B. M. Jones. The Measurement of Profile Drag by the Pitot Traverse Method. Reports and Memoranda No. 1688, British A.R.C., 1963.

8. R. Eppler (Francessa Neffgen, transl.). Laminar Airfoils for Reynolds Numbers Greater Than 4 x 10^6. B-819-35, 1969 (NTIS No. N69-28178).

9. H. Schliching. Boundary Layer Theory. McGraw Hill, 1979.

TABLE 1
Design Airfoil (FX61-163)

x/c	z/c (upper)	z/c (lower)
0	0	0
.00102	.00566	-.00248
.00402	.01234	-.00560
.00960	.01925	-.00907
.01702	.02641	-.01272
.02650	.03402	-.01656
.03802	.04175	-.02027
.05158	.04929	-.02412
.06694	.05690	-.02790
.08422	.06410	-.03160
.10330	.07110	-.03520
.12403	.07760	-.03870
.14643	.08370	-.04200
.17037	.08920	-.04510
.19558	.09420	-.04790
.22221	.09840	-.05040
.24998	.10190	-.05250
.27891	.10460	-.05420
.30861	.10640	-.05540
.33933	.10720	-.05610
.37056	.10730	-.05630
.40243	.10640	-.05590
.43469	.10460	-.05470
.46733	.10170	-.05290
.49997	.09780	-.05040
.53274	.09300	-.04720
.56525	.08770	-.04320
.59750	.08210	-.03850
.62938	.07640	-.03290
.66074	.07060	-.02690
.69133	.06500	-.02080
.72115	.05940	-.01520
.74995	.05390	-.01010
.77773	.04860	-.00580
.80435	.04350	-.00200
.82970	.03860	.00110
.85350	.03400	.00360
.87590	.02970	.00540
.89644	.02560	.00670
.91571	.02180	.00730
.93299	.01820	.00750
.94848	.01480	.00720
.96192	.01170	.00640
.97334	.00880	.00530
.98291	.00610	.00390
.99034	.00390	.00270
.99571	.00210	.00150
.99891	.00070	.00040
1.00000	0.00000	0.00000

TABLE 2
Flight Airfoil (T-6)

x/c	z/c (upper)	z/c (lower)
0	0	0
.00102	.00649	-.00435
.00422	.01071	-.00837
.00960	.01707	-.01172
.01702	.02410	-.01540
.02650	.03113	-.01941
.03802	.03883	-.02310
.05158	.04619	-.02711
.06694	.05389	-.03113
.08422	.06126	-.03481
.10330	.06828	-.03849
.12403	.07464	-.04218
.14643	.08100	-.04552
.17037	.08636	-.04887
.19558	.09138	-.05188
.22221	.09540	-.05466
.24998	.09874	-.05690
.27891	.10109	-.05891
.30861	.10310	-.06025
.33933	.10377	-.06092
.37056	.10377	-.06126
.40243	.10243	-.06126
.43469	.10008	-.06025
.46733	.09640	-.05858
.49997	.09205	-.05623
.53274	.08703	-.05289
.56525	.08134	-.04954
.59759	.07565	-.04619
.62938	.06962	-.04318
.66074	.06326	-.03916
.69133	.05757	-.03548
.72115	.05155	-.03213
.74995	.04619	-.02879
.77773	.04050	-.02544
.80435	.03548	-.02276
.82970	.03113	-.01908
.85350	.02577	-.01607
.87590	.02142	-.01305
.89664	.01741	-.01004
.91571	.01439	-.00703
.93299	.01172	-.00435
.94848	.00904	-.00268
.96192	.00669	-.00201
.98291	.00402	-.00134
1.00000	.00067	-.00067

TABLE 3
Model FX66-17AII-182 Airfoil

x/c (upper)	z/c	x/c (lower)	z/c
0	0	0	0
.00083	.00347	.00083	-.00516
.00166	.00563	.00166	-.00691
.00277	.00786	.00277	-.00856
.00388	.00966	.00388	-.00992
.00499	.01134	.00527	-.01136
.00585	.01259	.00641	-.01231
.01353	.02120	.01352	-.01676
.01781	.02521	.03588	-.02573
.02475	.03106	.05113	-.03040
.03467	.03841	.07643	-.03651
.05013	.04861	.10169	-.04131
.06090	.05510	.15067	-.04833
.07574	.06328	.20055	-.05321
.10199	.07608	.25032	-.05617
.15106	.09548	.30166	-.05775
.20035	.11042	.35047	-.05782
.25320	.12165	.40069	-.05597
.30311	.12819	.45007	-.05253
.35283	.13066	.49998	-.04772
.40185	.12902	.55056	-.04134
.45244	.12335	.59970	-.03396
.50043	.11506	.64952	-.02630
.55178	.10427	.70012	-.01892
.60095	.09328	.74995	-.01234
.65056	.08197	.79808	-.00737
.70137	.07028	.84898	-.00364
.74442	.06026	.89907	-.00133
.80012	.04737	.94758	-.00080
.84997	.03585	.97026	-.00095
.90009	.02433	.97832	-.00104
.94994	.01257	1.00000	-.00059
.97613	.00629		
.99033	.00285		
.99964	.00021		

TABLE 4
SMOOTH T-6 Airfoil

x/c (upper)	z/c	x/c (lower)	z/c
0	.00243	0	-.00243
.00224	.00882	.00087	-.00320
.00734	.01595	.00519	-.00806
.01502	.02355	.01327	-.01283
.02529	.03156	.02465	-.01775
.03787	.03975	.03896	-.02261
.05265	.04800	.05619	-.02750
.06951	.05602	.07567	-.03210
.08851	.06382	.09807	-.03651
.10964	.07133	.12272	-.04076
.13217	.07808	.14958	-.04489
.15663	.08420	.17836	-.04894
.18308	.08970	.20818	-.05252
.21115	.09453	.23979	-.05540
.24027	.09856	.27263	-.05768
.27058	.10164	.30685	-.05953
.33933	.10506	.33933	-.06072
.37056	.10495	.37056	-.06124
.40243	.10388	.40243	-.06100
.43469	.10188	.43469	-.05871
.46733	.09888	.46733	-.05669
.49997	.09515	.49997	-.05428
.53274	.09045	.53274	-.05138
.56525	.08516	.56525	-.04819
.59750	.07939	.59750	-.04474
.62938	.07311	.62938	-.04109
.66074	.06692	.66074	-.03749
.69133	.06075	.69133	-.03398
.72115	.05472	.72115	-.03059
.74995	.04884	.74995	-.02732
.77773	.04328	.77773	-.02419
.80435	.03791	.80435	-.02121
.82970	.03279	.82970	-.01841
.85350	.02806	.85350	-.01577
.87590	.02366	.87590	-.01333
.89664	.01963	.89664	-.01109
.91571	.01600	.91571	-.00905
.93299	.01284	.93299	-.00723
.94848	.01005	.94848	-.00565
.96192	.00762	.96192	-.00318
.98291	.00383	.98291	-.00117
1.00000	.00083	1.00000	-.00117

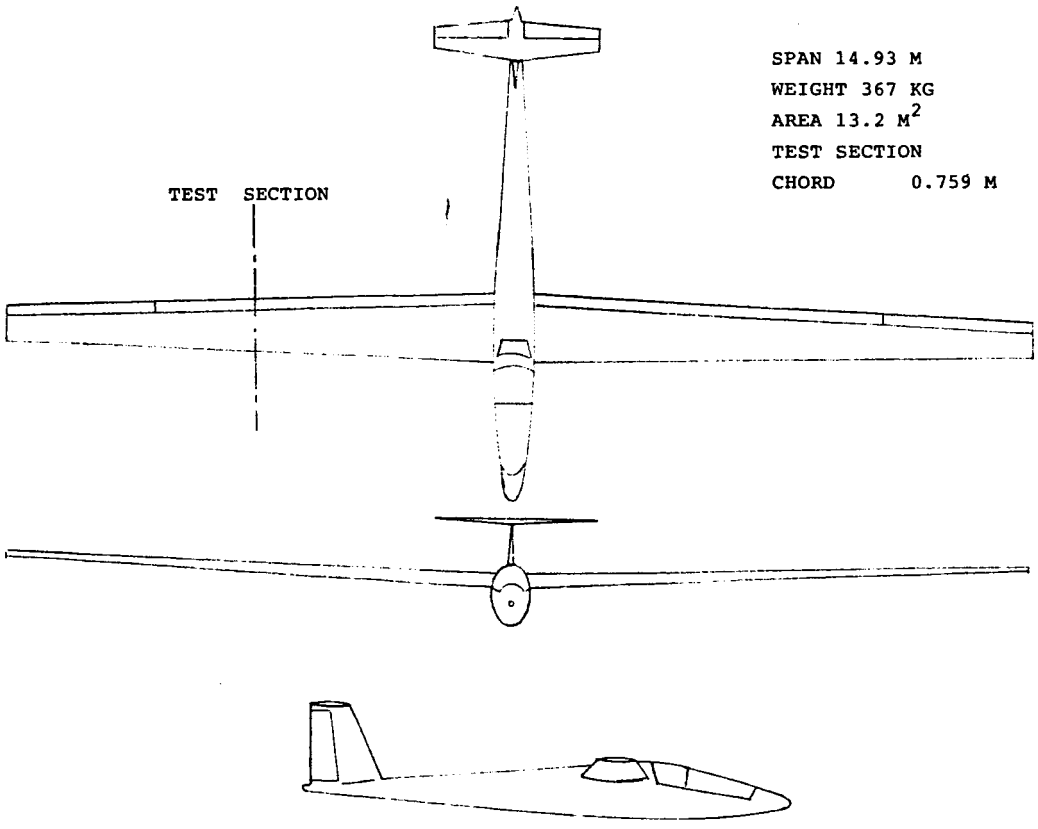

FIGURE 1. THREE VIEW OF T-6 SAILPLANE AND AIRFOIL SECTION

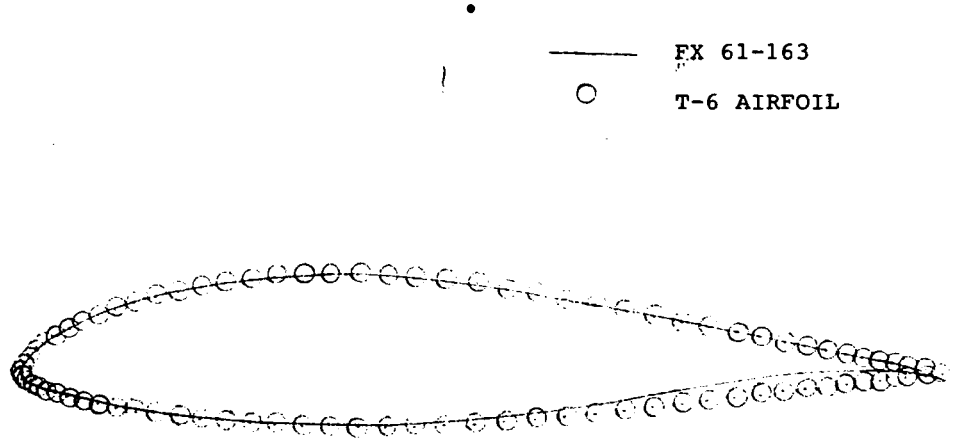

FIGURE 2. A comparison between the baseline FX 61-163 airfoil and the T-6 flight airfoil with 0^{o} flap deflection.

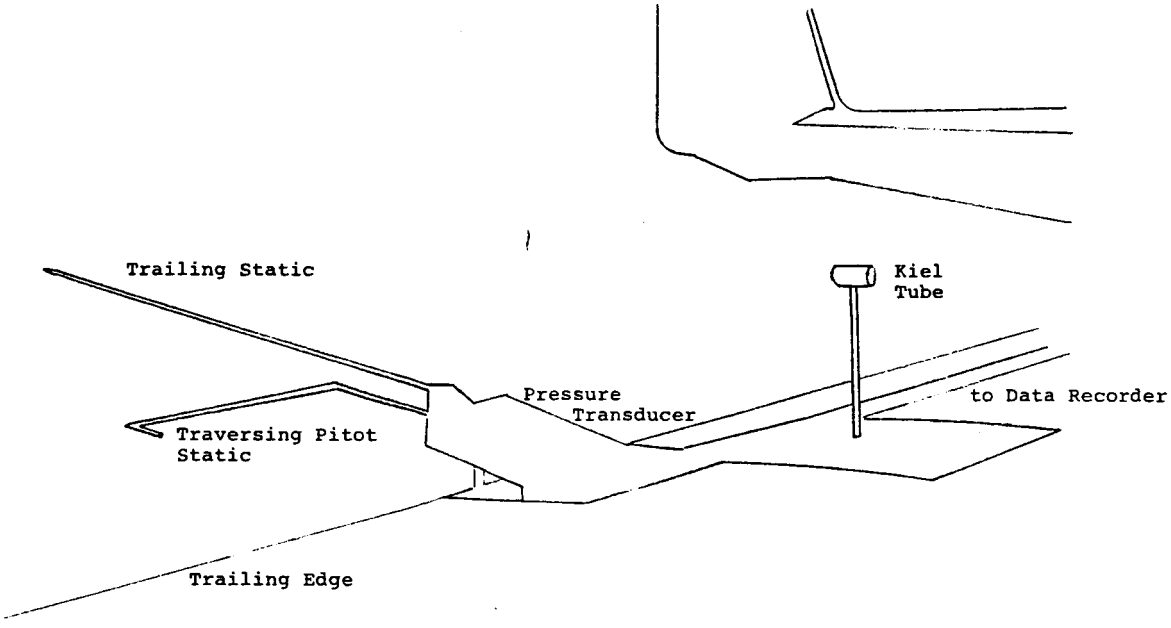

FIGURE 3. Wake rake installation on
T-6 sailplane.

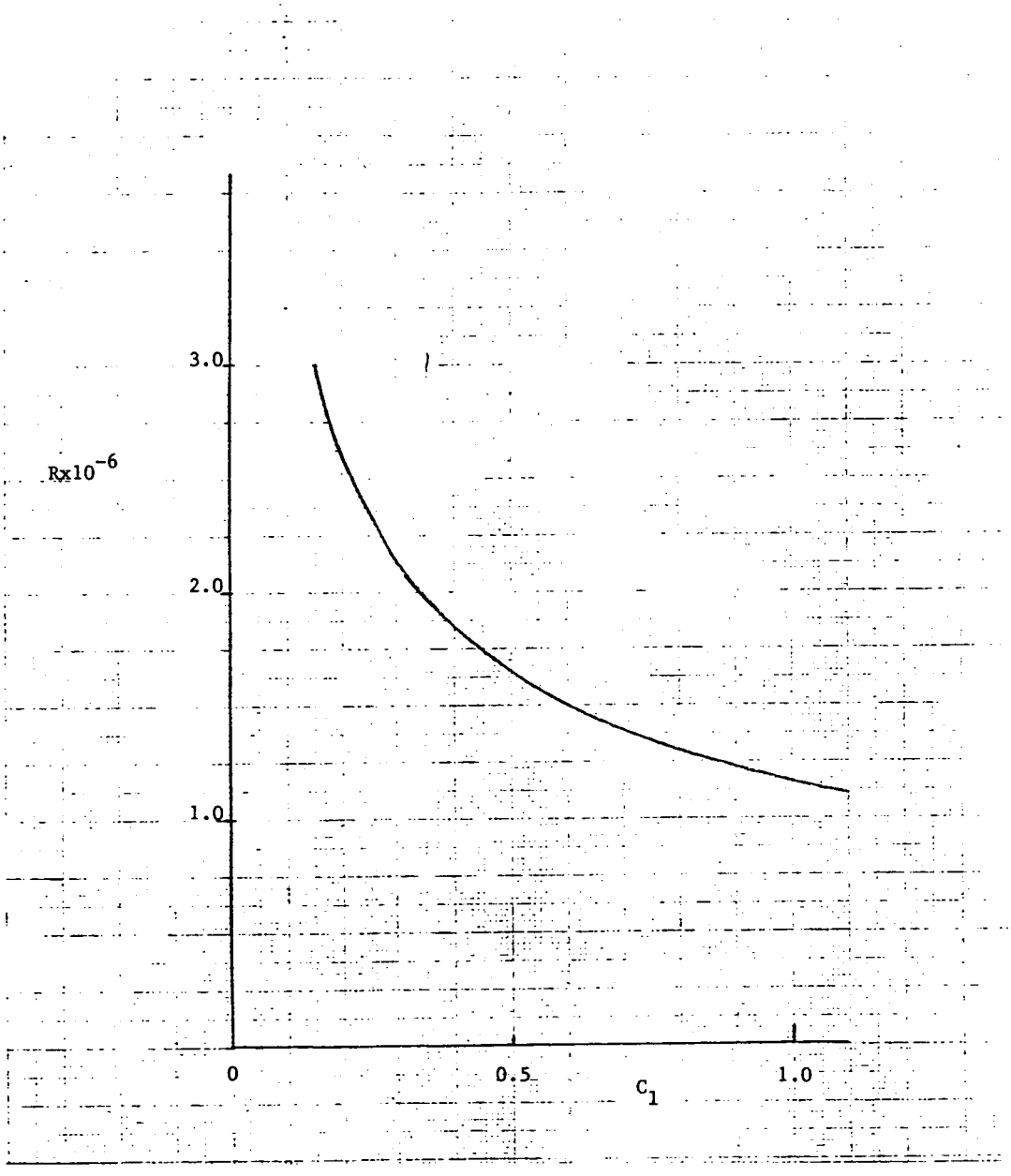

Fig. 4. - Section lift coefficient as a function of chord length Reynold's number for T-6 sailplane flight tests.

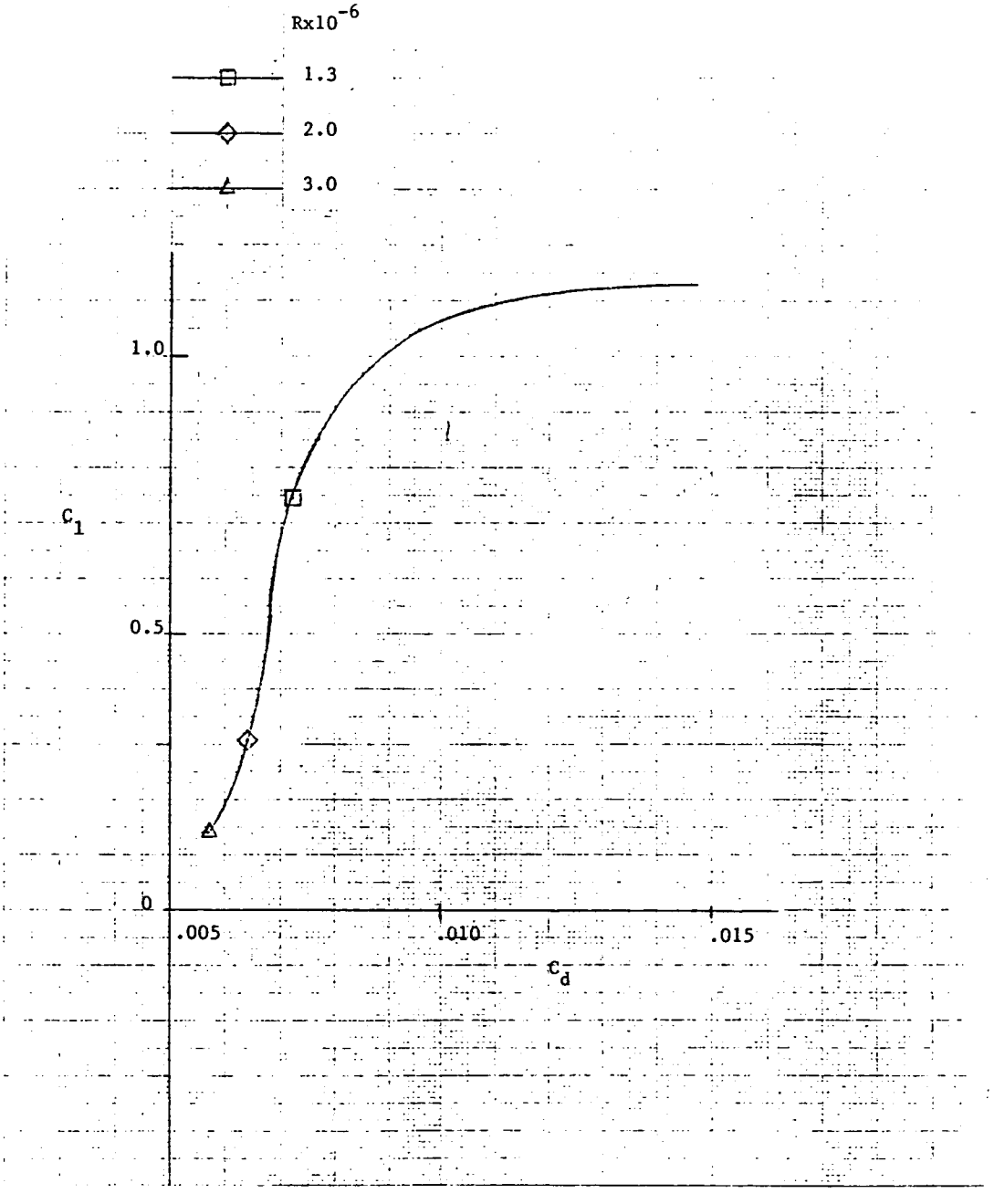

Fig. 5 - Polar for flight T-6 airfoil, C_l vs. C_d (Ref. 5.).

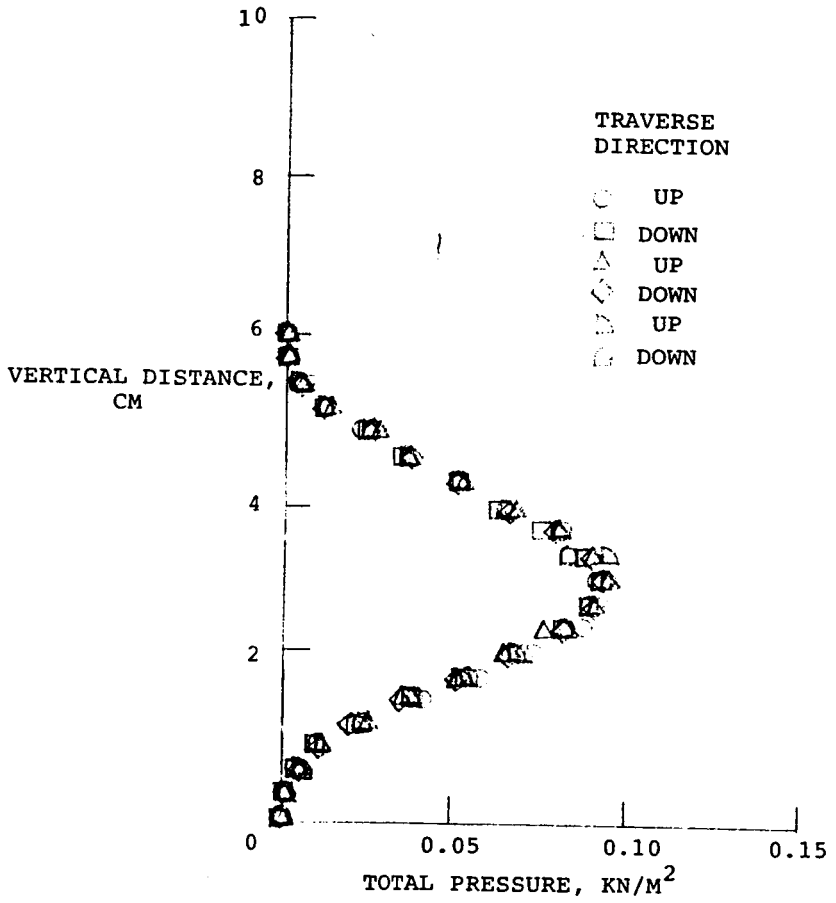

FIGURE Typical total pressure wake profiles. Six consecutive wakes; 0^{o} flap deflection; 44 knots; 0.31 kN/m^2 total pressure (reference 4.).

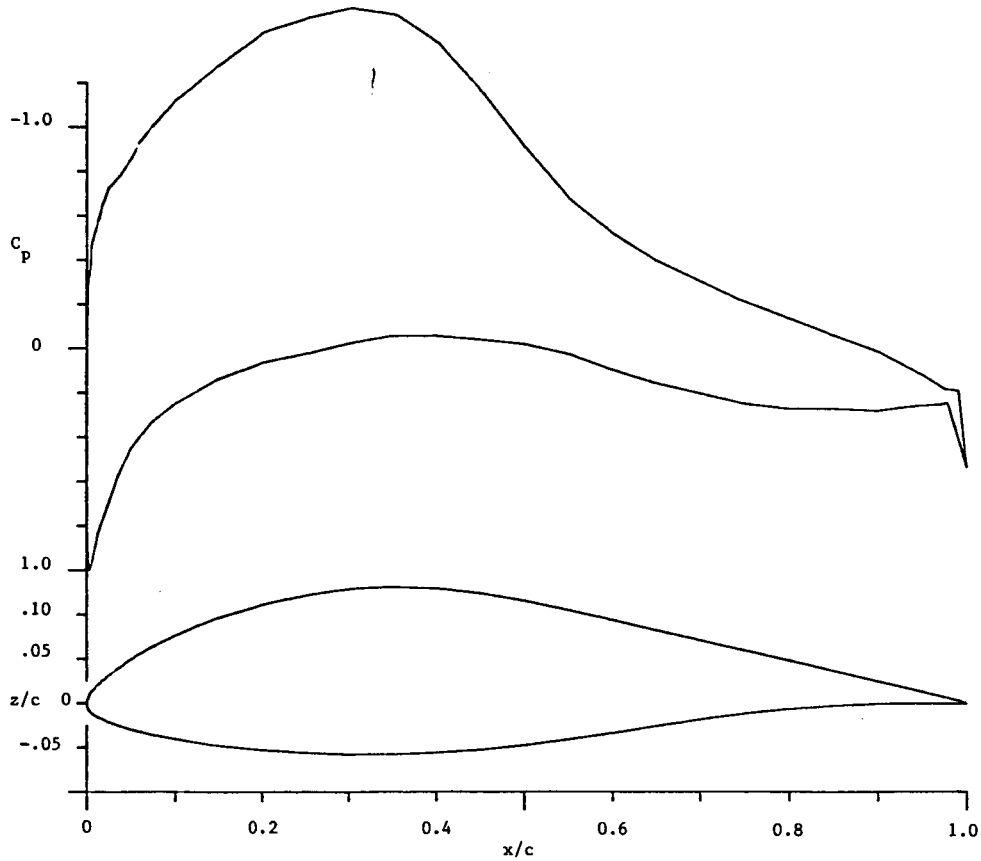

Fig. 7. - Pressure coefficients predicted for model FX66-17AII-182 airfoil by PROFILE. $\alpha = 4^{o}$

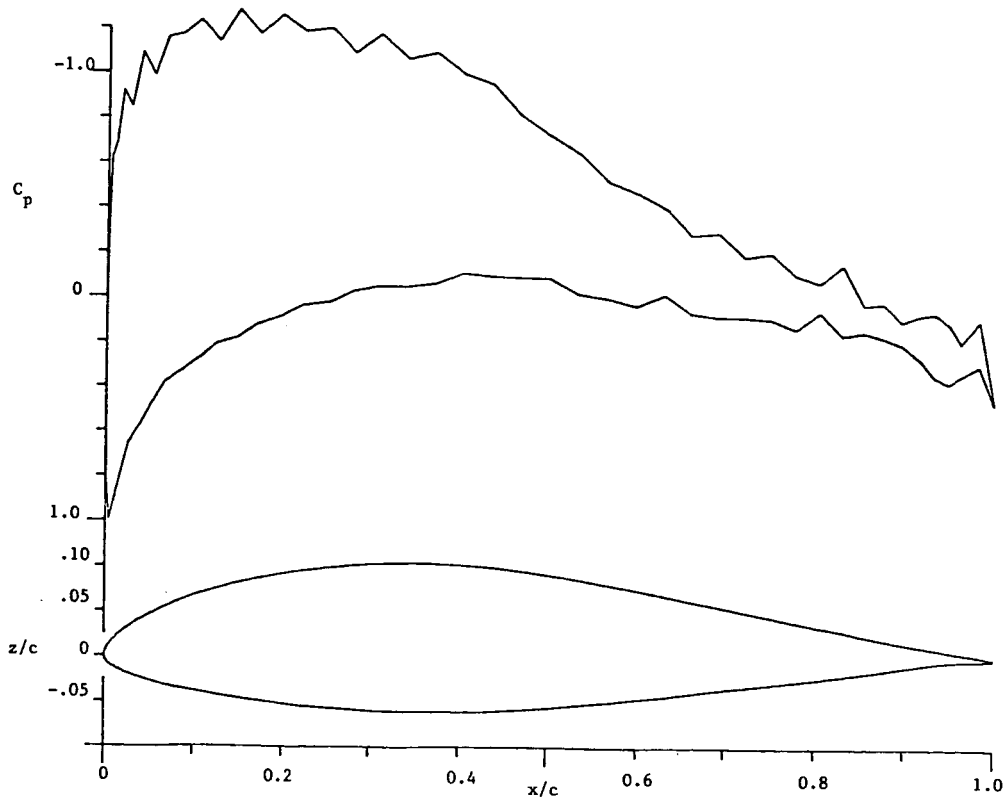

Fig. 8. - Pressure coefficients for flight airfoil predicted by PROFILE before smoothing (Ref. 5). $\alpha = 4^0$

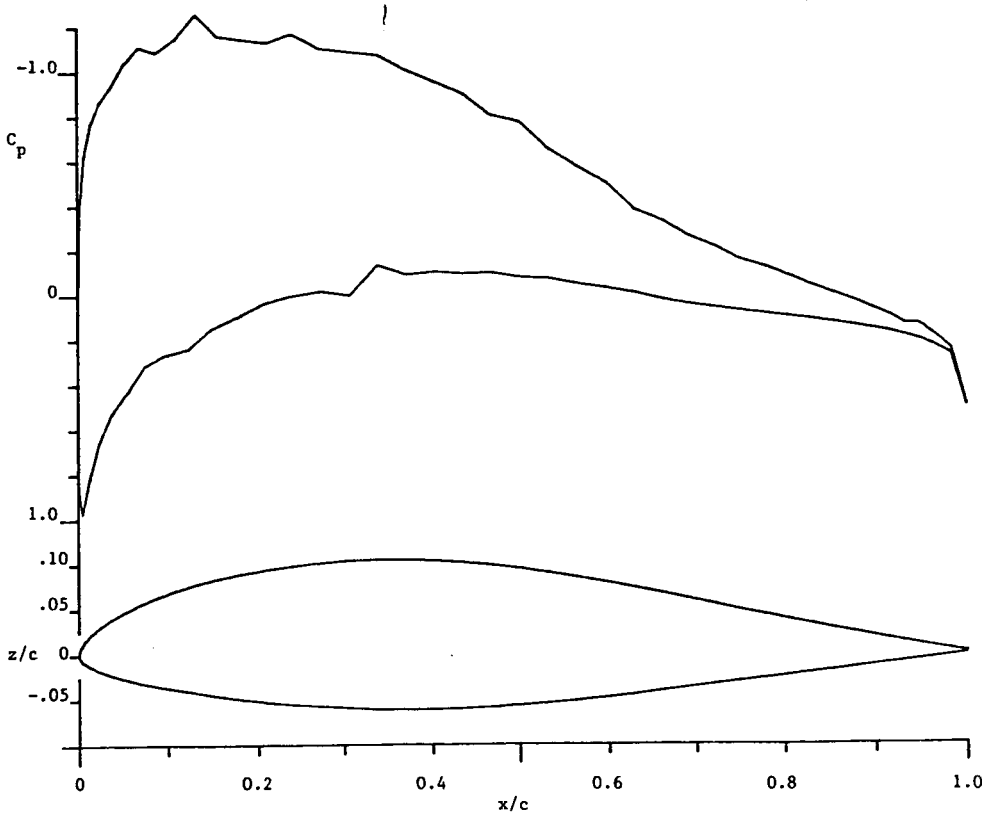

Fig. 9. - Pressure coefficients for flight airfoil predicted by PROFILE after modifications by smoothing routines SLOPE and MOD. $\alpha = 4^{o}$

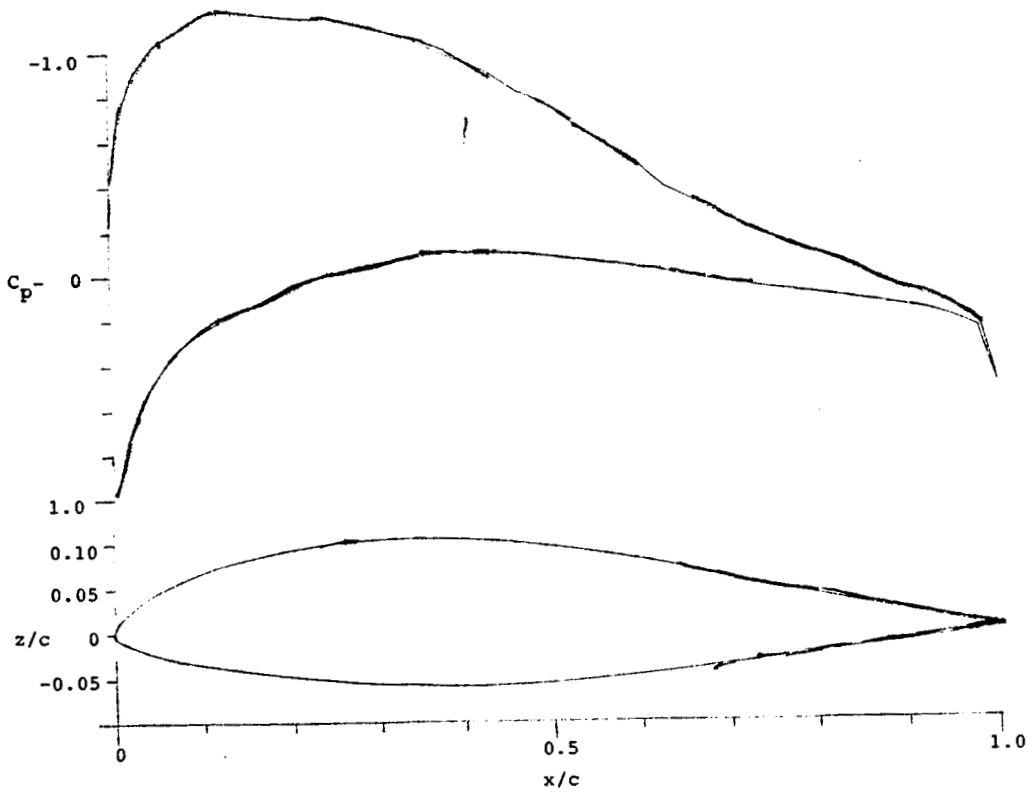

FIGURE Pressure coefficient (inviscid) for the flight airfoil at 4^{o} angle of attack.

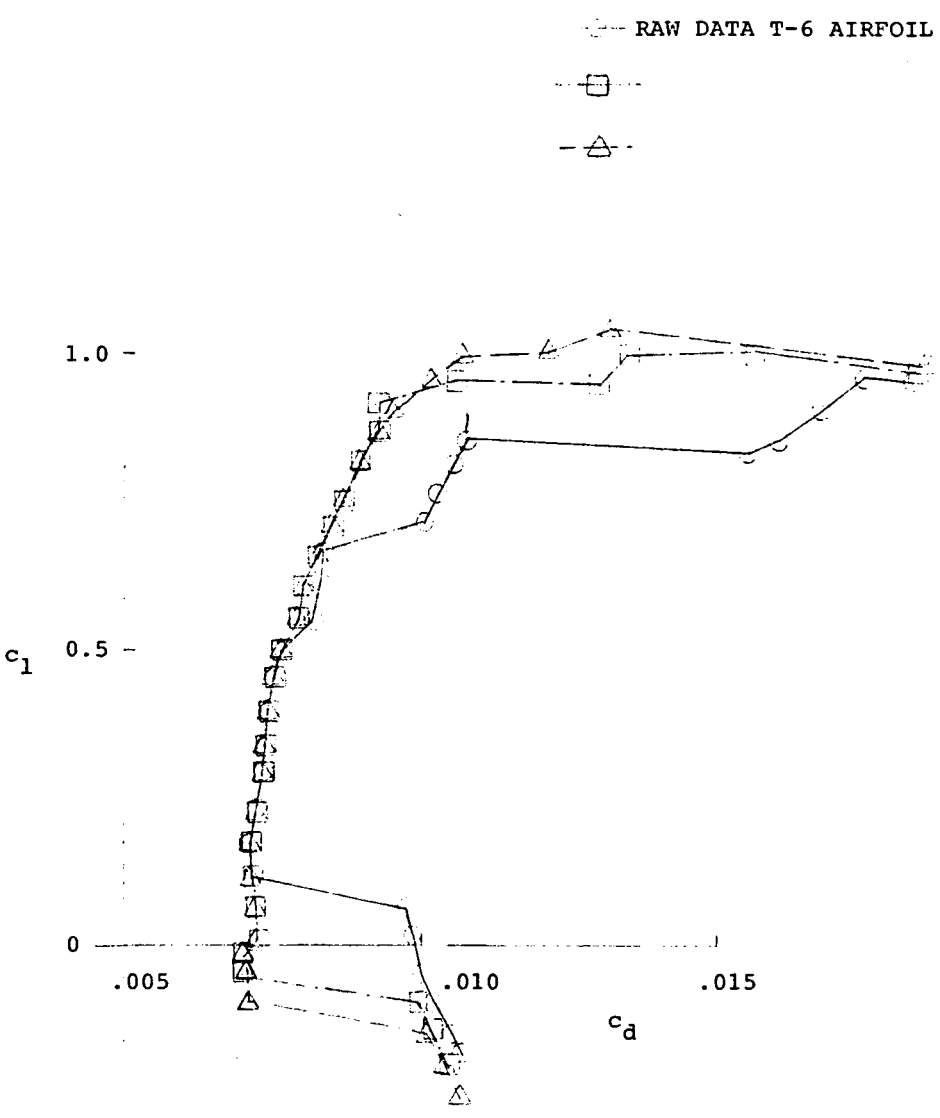

FIGURE A comparison of computed polars between the raw data T-6 airfoil and the

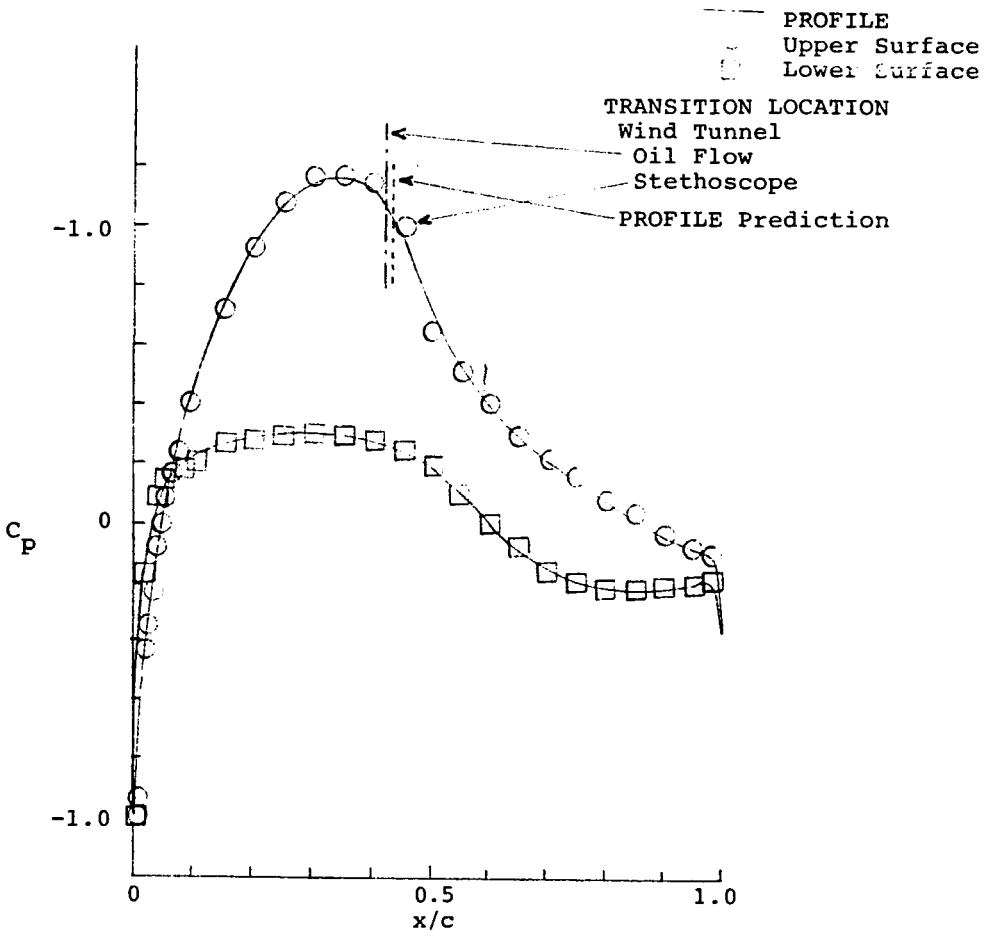

FIGURE Transition location and pressure coefficient comparison for FX 66-AII-182 airfoil in wind tunnel ($Re=1.5 \times 10^6$, $\alpha=0^o$, $c_l=0.4$) and on the PROFILE program ($Re=1.5 \times 10^6$, $\alpha=0^o$, $c_l=0.368$).

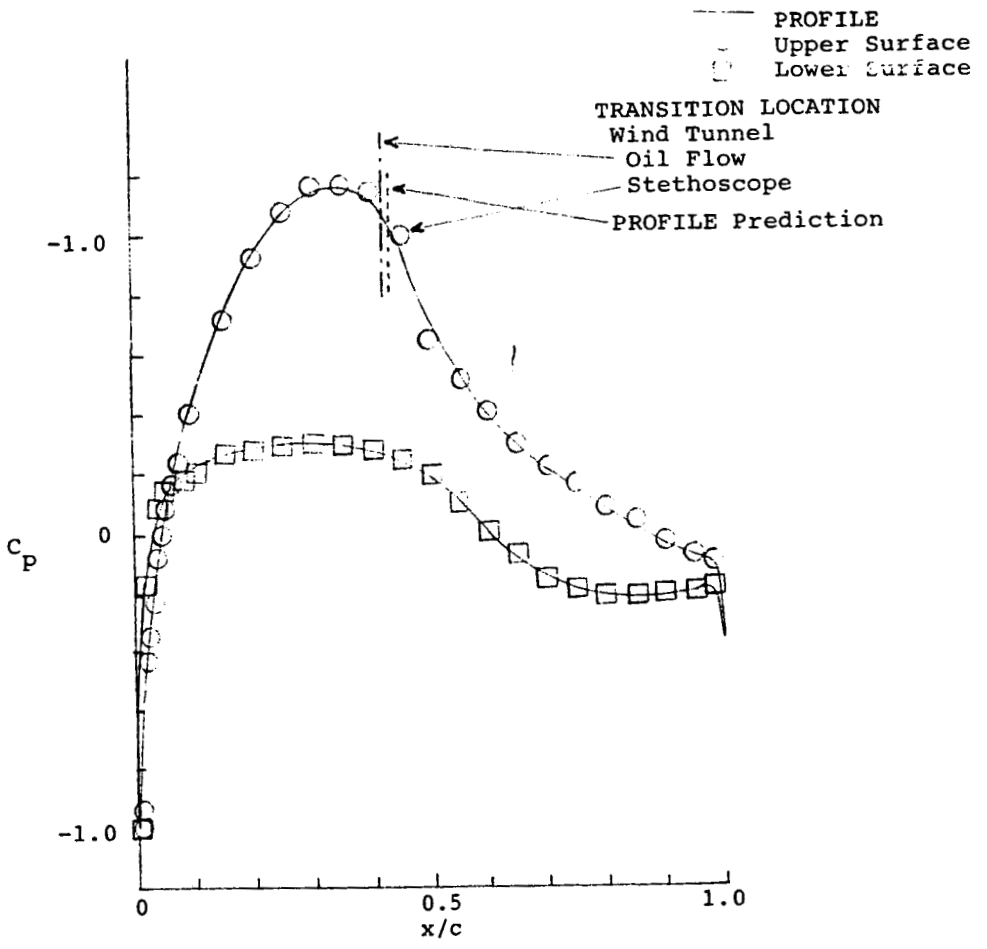

FIGURE Transition location and pressure coefficient comparison for FX 66-AII-182 airfoil in wind tunnel ($Re=1.5x10^6$, $\alpha=0^o$, $c_l=0.4$) and on the PROFILE program ($Re=1.5x10^6$, $\alpha=0^o$, $c_l=0.368$).

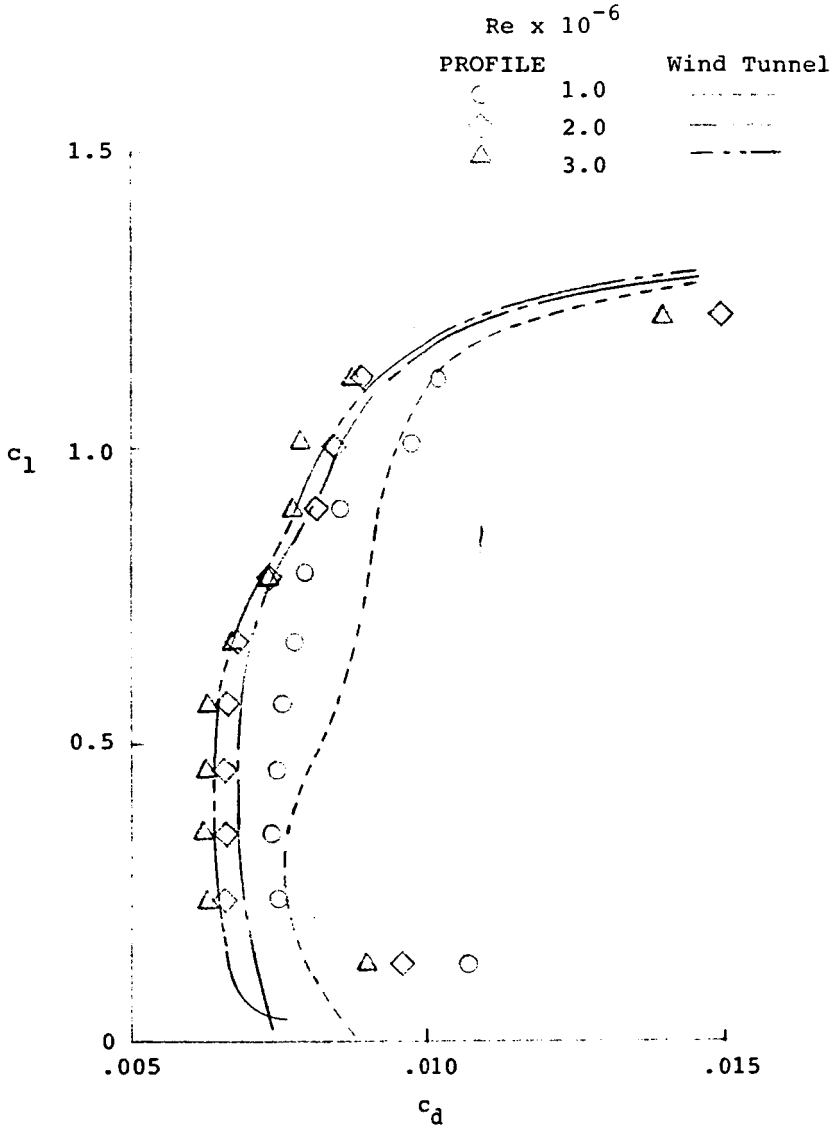

Figure A comparison between computed and wind tunnel data (Ref. 3) for the baseline airfoil.

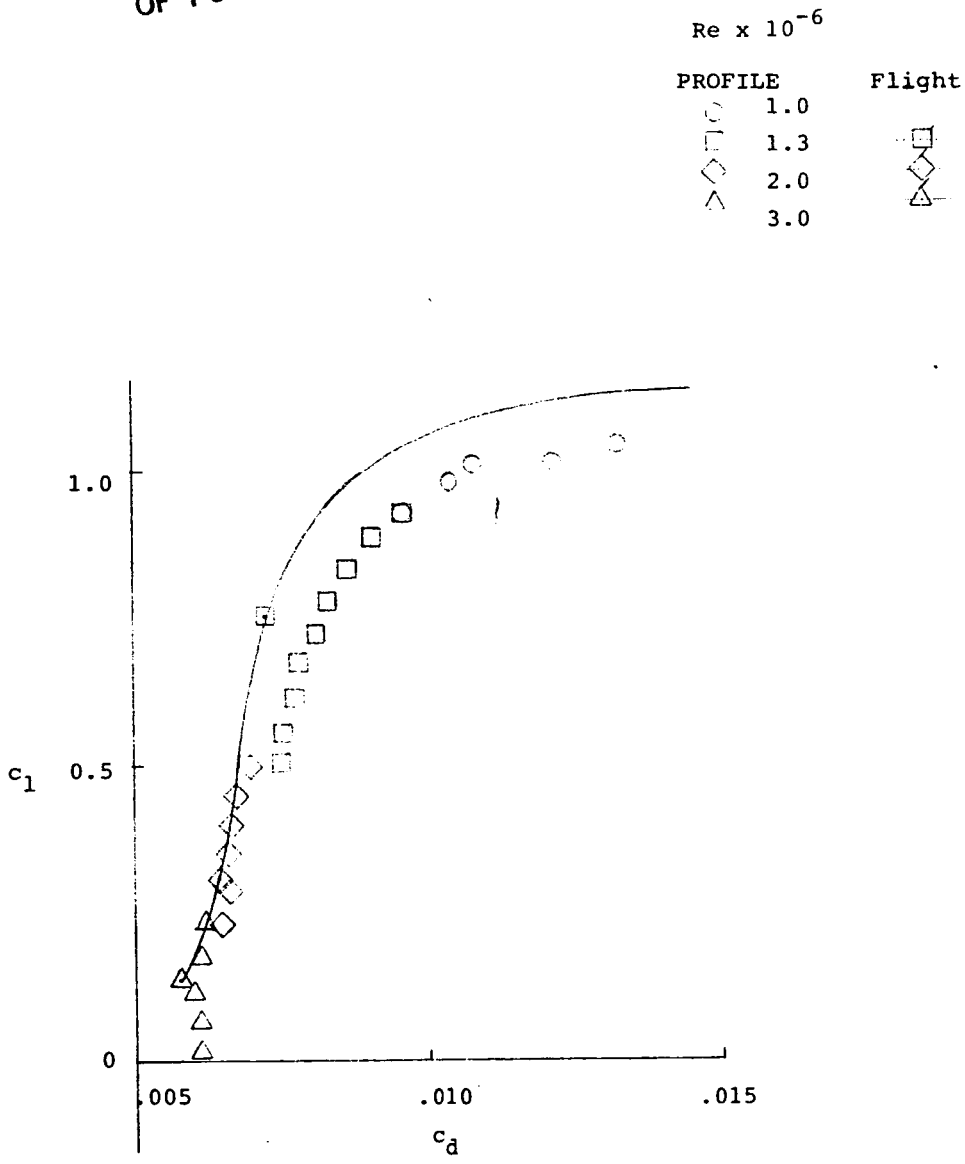

FIGURE A comparison between computed and flight data (Ref. 4) for the flight airfoil with 0° flap deflection.

CALIFORNIA POLYTECHNIC STATE UNIVERSITY
SAN LUIS OBIPO

BINDING INSTRUCTIONS

Bowers

1984

Low-Speed Airfoil Result Comparisons